Modeling process of embolization arteriovenous malformation on the basis of two-phase filtration model

A A Cherevko[1,2], T S Gologush[2], V V Ostapenko[1,2], I A Petrenko[3] and A P Chupakhin[1,2]

[1] Lavrentyev Institute of Hydrodynamics of the Siberian Branch of the Russian Academy of Sciences, Novosibirsk 630090, Russia
[2] Novosibirsk State University, Novosibirsk 630090, Russia
[3] Vladimir State University, Vladimir 60000, Russia

E-mail: cherevko@mail.ru, tatiana_06.08@mail.ru

Abstract. Arteriovenous malformation is a chaotic disordered interlacement of very small diameter vessels, performing reset of blood from the artery into the vein. In this regard it can be adequately modeled using porous medium. In this model process of embolization described as penetration of non-adhesive substance ONYX into the porous medium, filled with blood, both of these fluids are not mixed with each other. In one-dimensional approximation such processes are well described by Buckley–Leverett equation. In this paper Buckley–Leverett equation is solved numerically by using a new modification of Cabaret scheme. The results of numerical modeling process of embolization of AVM are shown.

1. Introduction

Arteriovenous malformation (AVM) is a pathological connection between arteries and veins. This anomaly leads to a direct bypass (reset) of blood from an arterial pool in the system of superficial and deep veins. The typical size of AVM amounts to centimeters. The most frequent cases, when AVM consists of vessels of very small diameter (0.01mm-0.9mm) and they almost completely fill the volume of AVM [1]. Cerebral AVM is a serious medical problem. More than half of the patients during life get haemorrhage, 10–30% of them die after the first haemorrhage, and from 10 to 20% of survivors are disabled. There are various treatments for AVM: microsurgical, endovascular and radiosurgical. Earlier embolization (endovascular method) was considered as an auxiliary method and used before removing or irradiating the AVM. The situation has changed with the advance of non-adhesive substance ONYX [2] and currently the endovascular methods are more popular. However, the danger of intraoperative rupture during embolization of AVM still exists. So development of modeling methods of embolization is an urgent problem [3, 4].

2. Modeling

2.1. Physical modeling

The typical AVM consists of large amount of strongly intertwined vessels of small diameter and so it can be considered as the porous medium with sufficient accuracy for modeling. In this case

Content from this work may be used under the terms of the Creative Commons Attribution 3.0 licence. Any further distribution of this work must maintain attribution to the author(s) and the title of the work, journal citation and DOI.
Published under licence by IOP Publishing Ltd

the movement of blood and non-adhesive substance ONYX through the AVM can be modeled as a two-phase filtration process, where the displaceable phase is blood and displacing phase is ONYX.

2.2. Mathematical modeling

In order to simplify the problem, we make the following assumptions. We assume that the AVM is a cylinder with length L, and that blood and non-adhesive substance are incompressible fluids. Within the one-dimensional approximation we consider all values as averaged over the cross section of the cylinder. Suppose that capillary forces can be neglected, and hence, the pressure in the phases is the same. Let the porosity of AVM is constant and equal to m. Denote by $S(x,t)$ saturation of blood. Let $k_i = k_i(S),\ i = b, e$, is the phase permeability for the blood and ONYX. Also, let $\mu_i,\ i = b, e$, is the viscosities of the blood and ONYX, which are constant. Because the characteristic time of embolization amounts to several tens of minutes, the change in values during the cardiac cycle is not taken into account. Also denote by $V = V(t)$ total flow volume for two phases, which is independent of x due to the assumption of impermeability of the lateral surface of the AVM. Then the equation for the saturation of blood inside the AVM during embolization can be written in the form of Buckley–Leverett [5, 6]:

$$m\frac{\partial S}{\partial t} + V(t)\frac{\partial\, b(S)}{\partial x} = 0, \tag{1}$$

where the function of the Buckley–Leverett

$$b(S) = \frac{k_b(S)/\mu_b}{k_b(S)/\mu_b + k_e(S)/\mu_e},$$

defining the allocation of the phase flows. It is determined on the interval $[0, 1]$. It is assumed that it satisfies the following conditions on this segment:

$$b(S) \in \mathbf{C}^1[0,1],\quad b(0) = 0,\ b(1) = 1,\quad b'(0) = b'(1) = 0,\quad b'(S) > 0\ \ \forall S \in (0,1).$$

By replacing $\theta = \frac{1}{m}\int_0^t V(\xi)d\xi$ the equation (1) can be simplified and reduced to the form:

$$\frac{\partial S}{\partial \theta} + \frac{\partial\, b(S)}{\partial x} = 0,$$

which will be further major for us.

2.3. Initial-boundary problem of embolization

At the initial moment AVM does not contain ONYX, that is $S(0,x) \equiv 1$. ONYX is injected into the AVM through the artery. We assume that the arterial part of AVM has the coordinate $x = 0$ and denote the saturation of blood on the arterial end by $g(\theta)$. According to medical indications, ONYX should never reach the venous end of AVM (high risk of rupture), that is always $S(\theta, L) = 1$.

Thus, the initial-boundary value problem has the form:

$$\frac{\partial S}{\partial \theta} + \frac{\partial\, b(S)}{\partial x} = 0, \tag{2}$$

$$S(0,x) = S_0(x),\quad x \in [0,L] \tag{3}$$

$$S(\theta,0) = g(\theta),\quad \theta \in (0,T]. \tag{4}$$

Moreover, due to the peculiarities of the process of embolization $S_0(x) \equiv 1$, and the moment of time T is determined from the condition that ONYX has reached the venous end of AVM.

3. Finite-difference scheme

For numerical solution of problem (2)–(4) we used the explicit second order CABARET scheme [7]. The main advantages of this scheme owe to the following property: in linear case this scheme is reversible in time and exact for two different Courant numbers $r = 0.5$ and $r = 1$. For this reason, the scheme possesses unique dissipative and dispersive properties [8]. In view of the special flux correction and certain constrains during approximation of initial data, the CABARET scheme is monotonic and strongly monotonic [9] at Courant numbers $r \leq 0.5$. Therefore, the value $r < 0.5$ is used in the computations described below. Moreover, the CABARET scheme has a compact stencil bounded by the size of one spatial-temporal cell of the difference grid.

The problem (2)–(4) is approximated by the two-time-level CABARET scheme [8] on a uniform rectangular grid

$$\{(x_j, \theta_n) : \ x_j = jh, \ j = \overline{0, J}; \quad \theta_n = n\tau, \ n = \overline{0, N} \ \}, \tag{5}$$

where $h = L/J$ and $\tau = T/N$ are constant mesh step in space and in time. The time step is determined according to the stability condition by the formula

$$\tau = \frac{zh}{\max\limits_{[0,1]} b'(S)} \ ,$$

where $z = 0.4$ is the safety factor. This scheme involves the flux variables $u_j^n = S(x_j, \theta_n)$ and the conservative variables $U_{j+1/2}^n = S(x_{j+1/2}, \theta_n)$, which are defined at integer x_j and half-integer $x_{j+1/2} = x_j + h/2$ spatial grid nodes, respectively.

Let u_j^n, $j = \overline{0, J}$ and $U_{j+1/2}^n$, $j = \overline{0, J-1}$ is the known numerical solution of problem (2)–(4) at the n-th time level θ_n; at $n = 0$, this is a grid approximation of the initial function $S_0(x)$. Based on the modified CABARET scheme, the numerical solution u_j^{n+1}, $U_{j+1/2}^{n+1}$ at the $(n+1)$-th time level θ_{n+1} is found in five stages. At the first stage, the difference equations

$$\frac{U_{j+1/2}^{n+1/2} - U_{j+1/2}^n}{\tau/2} + \frac{b_{j+1}^n - b_j^n}{h} = 0, \quad j = \overline{0, J-1},$$

where $b_j^n = b(u_j^n)$, are used to calculate the conservative variables $U_{j+1/2}^{n+1/2} = S(x_{j+1/2}, \theta_{n+1/2})$ at the half-integer time level $\theta_{n+1/2} = \theta_n + \tau/2$. At the second stage, the extrapolation

$$\tilde{u}_{j+1}^{n+1} = 2U_{j+1/2}^{n+1/2} - u_j^n, \quad j = \overline{0, J-1},$$

is employed to find the preliminary flux variables $\tilde{u}_j^{n+1}$, which are corrected as follows

$$\bar{u}_{j+1}^{n+1} = F\left(\tilde{u}_{j+1}^{n+1}, m_{j+1/2}^n, M_{j+1/2}^n\right), \quad j = \overline{0, J-1},$$

$$F(u, m, M) = \begin{cases} u, & m \leq u \leq M, \\ m, & u < m, \\ M, & u > M, \end{cases}$$

$$m_{j+1/2}^n = \min\left(u_j^n, U_{j+1/2}^n, u_{j+1}^n\right), \quad M_{j+1/2}^n = \max\left(u_j^n, U_{j+1/2}^n, u_{j+1}^n\right).$$

At the third stage, we use formulas

$$\bar{b}_j^{n+1/2} = b\left(\bar{u}_j^{n+1/2}\right), \quad \bar{u}_j^{n+1/2} = \frac{u_j^n + \bar{u}_j^{n+1}}{2}, \quad j = \overline{1, J},$$

for calculation of preliminary values $\bar{b}_j^{n+1/2}$ of numerical fluxes, which are corrected as follows

$$b_j^{n+1/2} = F\left(\bar{b}_j^{n+1/2}, \bar{m}_{j-1/2}^n, \bar{M}_{j-1/2}^n\right), \quad j = \overline{1, J},$$

$$\bar{m}_{j-1/2}^n = \min\left(b_{j-1/2}^n, \max(b_j^n, \varphi_{j-1/2}^n)\right), \ \bar{M}_{j-1/2}^n = \max\left(b_{j-1/2}^n, \min(b_j^n, \varphi_{j-1/2}^n)\right),$$

$$b_j^n = b(u_j^n), \quad b_{j-1/2}^n = b(U_{j-1/2}^n), \quad \varphi_{j-1/2}^n = \frac{U_{j-1/2}^n - u_{j-1}^n}{r} + b_{j-1}^n, \quad r = \frac{\tau}{h}.$$

The left boundary numerical flux $b_0^{n+1/2}$ is defined from boundary condition (5) under the formula

$$b_0^{n+1/2} = b(g(\theta_{n+1/2})).$$

At the fourth stage, the difference equations

$$\frac{U_{j+1/2}^{n+1} - U_{j+1/2}^n}{\tau} + \frac{b_{j+1}^{n+1/2} - b_j^{n+1/2}}{h} = 0, \quad j = \overline{0, J-1},$$

are used to calculate the conservative variables $U_{j+1/2}^{n+1} = S(x_{j+1/2}, \theta_{n+1})$ at the $(n+1)$-th time level $\theta_{n+1} = \theta_n + \tau$. At the fifth stage, we restore flux variables

$$\hat{u}_j^{n+1} = 2b^{-1}\left(b_j^{n+1/2}\right) - u_j^n, \quad j = \overline{1, J-1},$$

where b^{-1} is the function inverse to b, which then is corrected as follows

$$u_j^{n+1} = F\left(\hat{u}_j^{n+1}, m_j^{n+1}, M_j^{n+1}\right), j = \overline{1, J-1},$$

$$m_j^{n+1} = \min\left(U_{j-1/2}^{n+1}, U_{j+1/2}^{n+1}\right), \quad M_j^{n+1} = \max\left(U_{j-1/2}^{n+1}, U_{j+1/2}^{n+1}\right).$$

The boundary flux variables at $j = 0, J$ are set by formulas

$$u_0^{n+1} = b(g(\theta_{n+1})), \quad u_J^{n+1} = \bar{u}_J^{n+1},$$

first of them follows from boundary condition (5). As a result we have the finite-difference solution on the $(n+1)$-th time level.

By analogy to paper [10], it is possible to show that the offered modification of the CABARET scheme is monotonous [11] that provides its high resolution at shock capturing calculation.

4. Model calculations

In order to test the suitability of the method for the calculation tasks of embolization, the essential moments of embolization process were modeled in our numerical experiments.

4.1. Model function of Buckley–Leverett and exact solutions

In the calculations Buckley–Leverett function was used and it was defined by analytical :

$$b(S) = \sin^2\left[\frac{\pi S}{2}\right].$$

The plot of this function is shown in Figure 1. Prescribed in such way, the Buckley–Leverett function allows to construct exact solutions of initial-boundary value problem in some cases. It

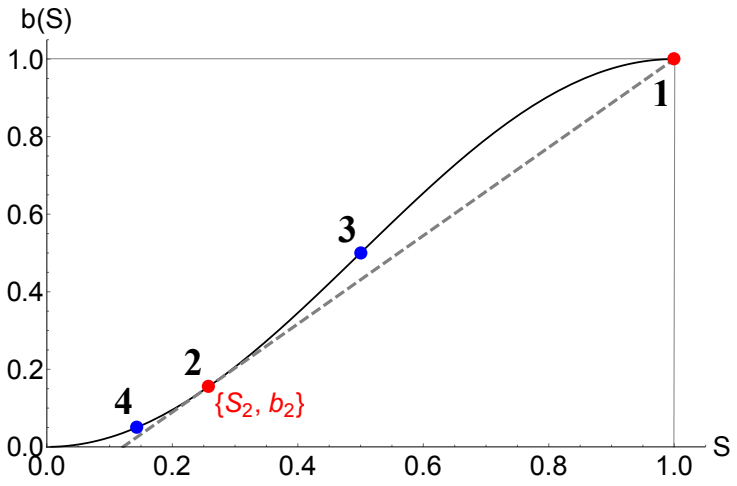


Figure 1. The model form of the Buckley–Leverett function.

must be noted that since the function of Buckley–Leverett is not convex, and the problem is hyperbolic, then compression shock waves as well rarefaction shock waves may be formed in the solution.

Let us consider the behaviour of the solution at the start of embolization. For simplicity, assume that at moment of time $\theta = 0$, ONYX is introduced and, due to it, blood saturation immediately reduced to a value $g_0 < 1$. And this concentration of ONYX at the input is being supported throughout the all time of modeling. Because the sound speed $b'(S)$ is equal to zero, where $S(x, 0) = 1$, no continuous movement is possible, thus information from $x = 0$ can not be spread inside the domain. The only option is the flow with rarefaction shock wave.

There are two qualitatively different cases. Point 2 with coordinates (S_2, b_2) plays an important role on the plot of the function $b(S)$. It is defined as the point of tangency of the curve $b(S)$ and straight line, which passes through the point 1 with coordinates $(1, 1)$. The point 1 corresponds to the initial state before the shock wave.

If condition behind the shock wave is the point 3 on Figure 1, which lies above the point 2, stable shock wave $1 - 3$ is formed, in accordance with the O. A. Oleinik criterion of shock wave stability [12]. The solution consists of two constant values, connected by a running gap. Two families of characteristics come on the shock wave, one is from x-axis and the other is from θ-axis.

This solution is given by the following equation:

$$S = \begin{cases} 1, & x \geq \theta \left(b(S_0) - b(g_0)\right) / \left(S_0 - g_0\right) \\ g_0, & x < \theta \left(b(S_0) - b(g_0)\right) / \left(S_0 - g_0\right) \end{cases}$$

If condition behind the shock wave is the point 4, which lies below the point 2, the shock wave $1-4$ will be unstable in accordance with the O. A. Oleinik criterion. Such wave at the time $\theta > 0$ decomposes into shock wave $1 - 2$ with lower intensity and self-similar solution abutting to it (centred rarefaction wave).

The analytical expression for this case has the form:

$$S = \begin{cases} 1, & x \geq b'(S_2)\theta \\ (b')^{-1}(x/\theta), & b'(g_0)\theta < x < b'(S_2)\theta \\ g_0, & x \leq b'(g_0)\theta \end{cases}$$

4.2. Results of numerical modeling
Calculations were carried out on a rectangular grid with constant steps in time and space. The number of partitions in space is equal to 100 points, the number of partition points in time takes the value 300 to 400 in different cases. Courant number, which is equal to $z = 0.4$, was chosen for calculations.

The results are shown in the figures of two types:
1) Plots of conservative quantities U_j^n — where calculated values U_j^n are depicted as circles, and for some cases the line corresponding to the exact solution is drawn.
2) Plots on a plane (x, θ), on which contour lines U_j^n (corresponding to characteristics) and shock waves are shown.

4.2.1. Constant boundary condition $S \equiv g_0 > S_2$. Without loss of generality, we assume $g_0 = 0.5$. The calculation results are shown in Figure 2. It is seen that the calculation reproduces strong discontinuity of solution well and no numerical oscillations near this gap are observed.

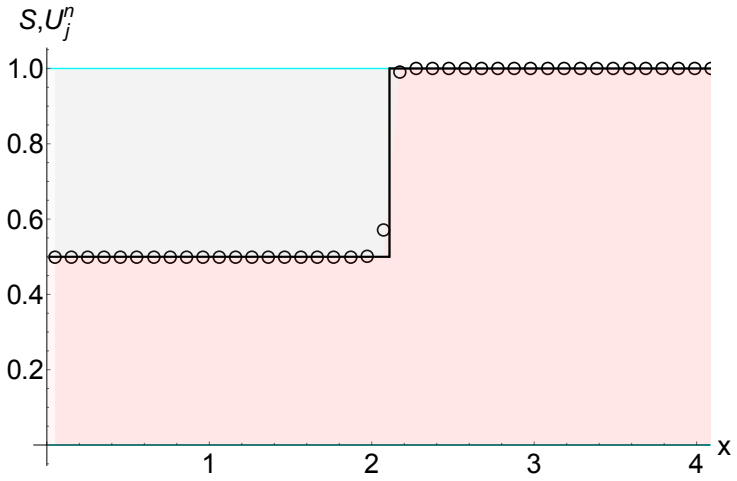


Figure 2. Numeric (circles) and exact (line) solutions for the case $g_0 = 0.5$ at time $\theta = 2.5$.

4.2.2. Constant boundary condition $S \equiv g_0 < S_2$. Condition $g_0 = 0.1$ is selected for calculation. The calculation results are shown in Figure 3. The calculation sufficiently reproduces the discontinuity decay, both in the shock region and the area of centred rarefaction wave.

4.2.3. The collision of two shock waves. Formation of shock waves is possible not only at the first moment of time, but also later, even in the case of continuous boundary conditions. As an example we consider the following boundary condition:

$$g_0 = \begin{cases} 0, & \theta \leq 2 \\ (\theta - 2)/8, & 2 < \theta < 10 \\ 1, & \theta \geq 10. \end{cases}$$

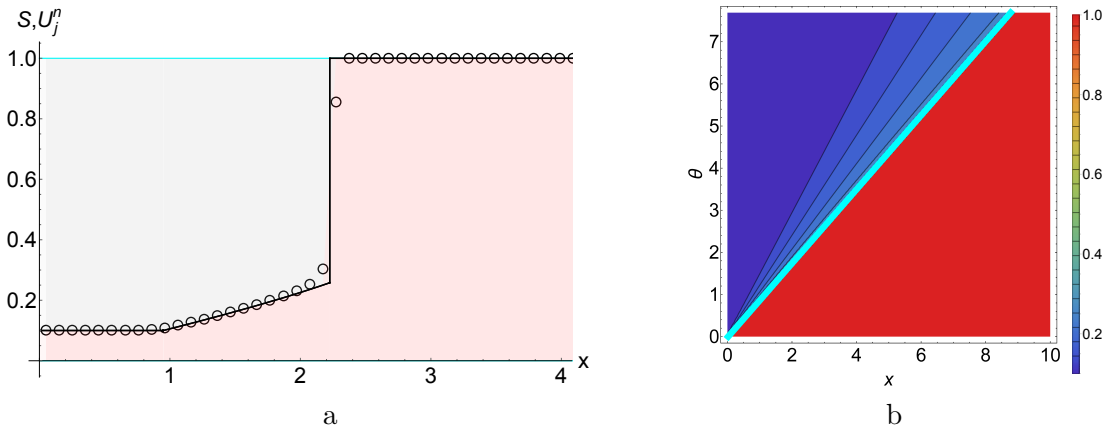


Figure 3. The case $g_0 = 0.1$. **a** – Numeric (circles) and exact (line) solutions at time $\theta = 2.5$. **b** – Result of simulation in (x, θ) plane with exact solution shock wave line (cyan).

In this case at the moment of time $\theta = 2$ a compression shock wave is formed. It catches up a rarefaction shock wave (formed at $\theta = 0$) and merges with it. As result a shock wave of lower intensity is formed. The exact solution is rather complicated, thus we consider only a numeric solution. Corresponding calculation is shown in Figures 4, 5a.

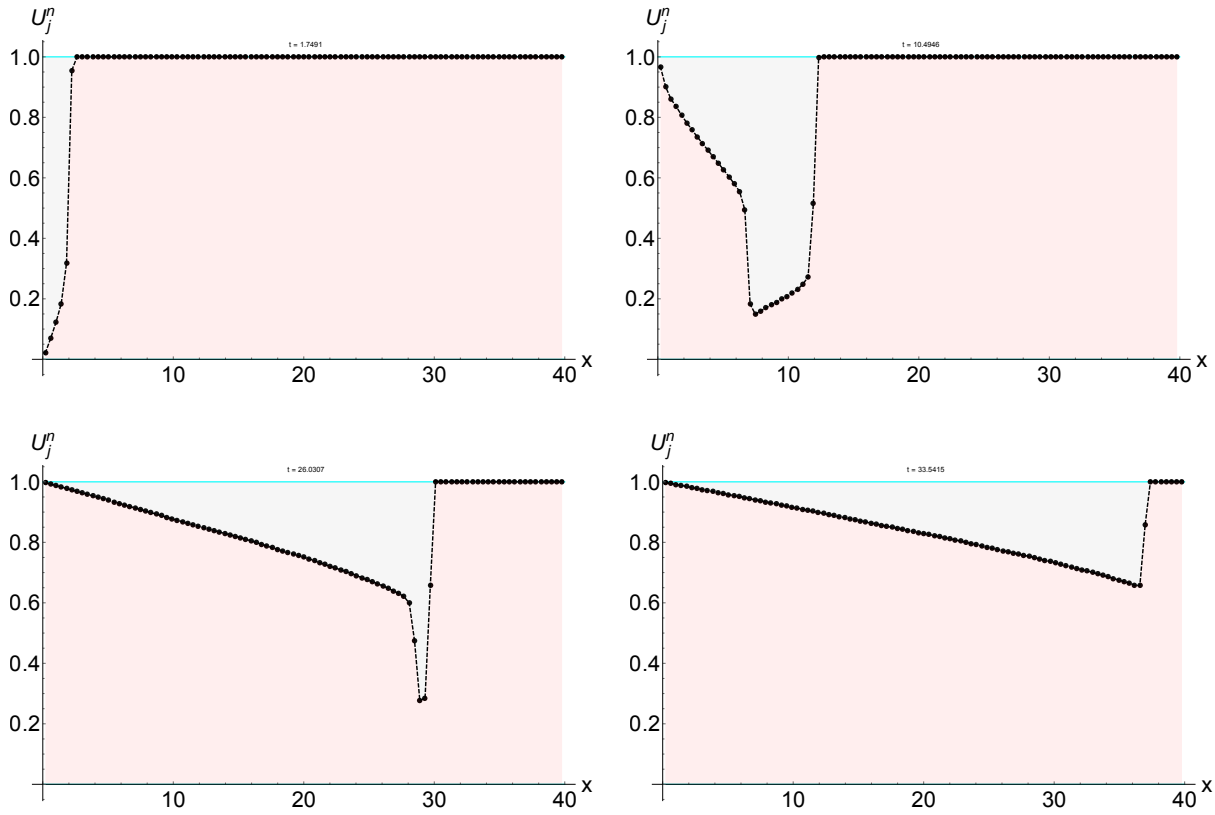


Figure 4. The collision of two shock waves. Successive stages of the process development. Black points – numerical result, dashed line – its linear interpolation.

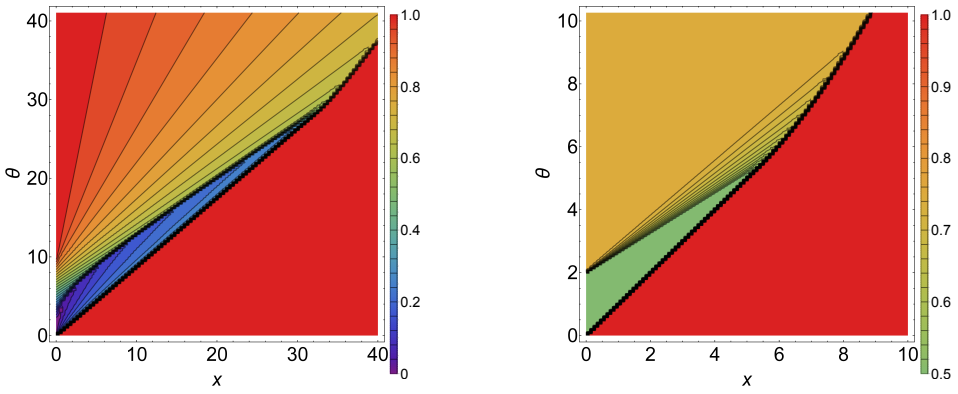


Figure 5. Result of simulation in (x, θ) plane. **a** – the collision of two shock waves, **b** – complicated flow with one shock wave. Shock wave curves roughness is not result of computation, but result of pre-plot interpolation.

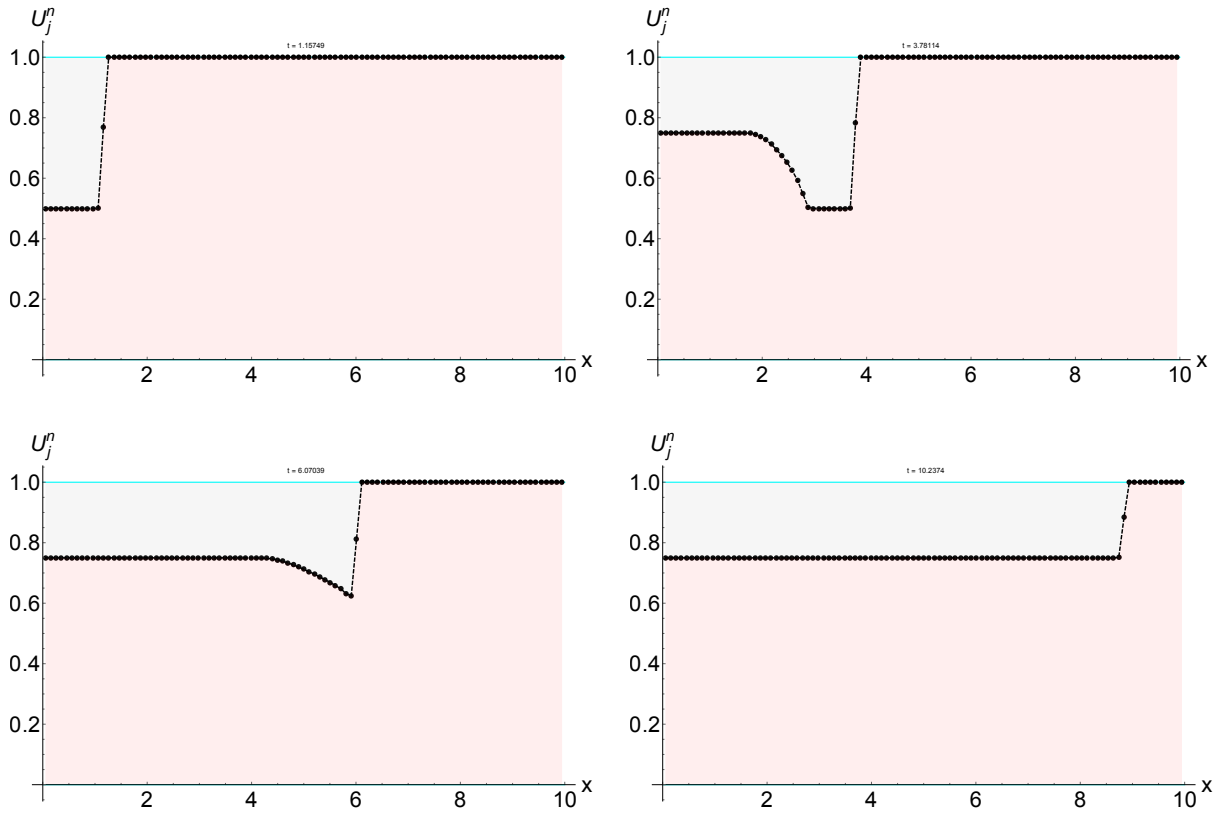


Figure 6. Complicated flow with one shock wave. Successive stages of the process development. Black points – numerical result, dashed line – its linear interpolation.

4.2.4. Complicated flow with one shock wave. Even discontinuous boundary conditions not always lead to the appearance of discontinuity in the solution. We choose function $g(\theta)$ as:

$$g_0 = \begin{cases} 0.5, & \theta < 2 \\ 0.75, & \theta \geq 2 \end{cases}$$

The shock wave formed by the discontinuity in the boundary conditions is unstable, so it breaks up into a centred compression wave when $\theta > 0$. Only numerical simulation is carried out in this case. The results corresponding to the calculation are shown in Figures 5b, 6.

5. Conclusions

The monotonous by Godunov version of Cabaret scheme, proposed by the authors, well reproduces the essential features of discontinuous flows, arising in the embolization problems. It can be used for further study on the process of AVM embolization.

Acknowledgments

The study was completed thanks to the support of Russian Foundation for Basic Research (project No. 14-01-00036).

References

[1] Klimov A B, Ryabuhin V E, Orlov K Y and Krilov V V 2012 *Surgery of the Cerebral Aneurysms* **3** 231–68
[2] Krivoshapkin A L et al 2013 *Bulletin SB RAMS* **33** 65–73
[3] Chupahin A P, Cherevko A A, Khe A K, Telegina N Y, Krivoshapkin A L, Orlov K Y, Panarin V A and Baranov V I 2012 *Patologija krovoobrashenija i kardiohirurgija (in russian)* **16** 27–31
[4] Panarin V A, Orlov K Y, Krivoshapkin A L, Chupahin A P, Cherevko A A, Khe A K, Telegina N Y and Baranov V I 2012 *Patologija krovoobrashenija i kardiohirurgija (in russian)* **16** 39–43
[5] Buckley S E and Leverett M C 1942 *Soc. Pertrol. Eng. J.* **146** 107–16
[6] Basniev K S, Kochina N I and Maximov M V 1993 *Undeground Hydromechanics* (Moscow: Nedra)
[7] Goloviznin V M 2005 *Dokl. Math.* **72** 619–23
[8] Karabasov S A and Goloviznin V M 2009 *J. Comp. Phys.* **228** 7426–51
[9] Ostapenko V V 2012 *Comput. Math. Math. Phys.* **52** 447–60
[10] Zyuzina N A and Ostapenko V V 2016 *Dokl. Math.* **93** 69
[11] Godunov S K 1959 *Mat. Sb. (in Russian)* **47** 271–306
[12] Oleinik O A 1959 *Uspehi Mat. Nauk (in Russian)* **14** 159–164